

# Topological Superconductors in Correlated Chern Insulators

Ying Liang,<sup>1</sup> Jing He,<sup>1</sup> Ya-Jie Wu,<sup>1</sup> Ying-Xue Zhu,<sup>1</sup> and Su-Peng Kou<sup>1,\*</sup>

<sup>1</sup>*Department of Physics, Beijing Normal University, Beijing, 100875, P. R. China*

In this paper, we realize a topological superconductor (TSC) in correlated topological insulator - the interacting spinful Haldane model. We consider the electrons on the Haldane model with on-site negative-U interaction and then study its properties by mean field theory and random-phase-approximation (RPA) approach. We found that in the intermediate interaction region, the ground state becomes a TSC with the Chern number  $\pm 2$ . We also study its edge states and the zero modes of the  $\pi$ -flux.

## I. INTRODUCTION

Different from the traditional superconductor (SC), topological superconductor (TSC) always has the topologically-protected gapless Majorana edge states[1]. For TSCs, people cannot use the local order parameter to characterize them. Instead, it is the topological invariant that plays the role to classify the topological properties of TSCs. According to the characterization of "ten-fold way" from random matrix[2-4], there exist three types of TSCs in two dimensions: D-type chiral TSC, of which the topological invariant is the Chern number[5], C-type chiral TSC, of which the topological invariant is also the Chern number and DIII-type TSC[5], of which the topological invariant is  $\mathbb{Z}_2$  topological invariant. For the D-type chiral TSC, a typical example is two dimensional  $p_x \pm ip_y$  chiral  $p$ -wave superconductor. This TSC has exotic topological properties, such as the topological protected chiral Majorana edge states and Majorana zero mode on  $\pi$ -flux[1]. In particular, a  $\pi$ -flux with Majorana mode becomes non-Abelian anyons due to its non-Abelian statistics[5]. To realize a D-type TSC people always consider the system with s-wave pairing SC and strong spin-orbital coupling in strong Zeeman field[6, 7]. For the C-type chiral TSC, a typical example is two dimensional  $d_x \pm id_y$  chiral  $d$ -wave superconductor. This TSC also has the topological protected chiral edge states and zero mode on  $\pi$ -flux[5]. However, till now people cannot realize the  $d_x \pm id_y$  chiral  $d$ -wave superconductor in a physical system.

In this paper we will show another road to realize a TSC in an interacting topological insulator - the interacting spinful Haldane model. The Haldane model is a lattice model that illustrates integer quantum Hall effect without Landau levels[8]. We consider the electrons on the Haldane's model with on-site negative-U interaction and then study its properties by mean field theory and RPA approach. We found that in the intermediate interaction region, the ground state becomes a TSC with the Chern number  $\pm 2$ . For the ground state there is a local order parameter and the elementary excitations are gapless phase fluctuations and gapped quasi-particle (an

electron or a hole). To characterize its topological properties, we study its edge states and the zero modes on the  $\pi$ -flux. Thus we propose that the s-wave topological superconductor/superfluid may be realized by putting two-component (two pseudo-spins) interacting fermions on a honeycomb optical lattice.

The paper is organized as below. In Sec. II, we start with the Hamiltonian of the interacting spinful Haldane model on the honeycomb lattice. In Sec. III, We calculate the superconducting order parameter with mean field approach and get a global phase diagram at zero temperature. In Sec. IV, we discuss the topological properties of the TSC, including the zero modes of the  $\pi$ -flux and the edge states. In Sec. V, we calculate the phase stiffness of the TSC. In Sec. VI, we discuss the physical realization of the s-wave topological superconductor/superfluid in a honeycomb optical lattice. Finally, the conclusions are given in Sec. VII.

## II. THE SPINFULL HALDANE MODEL WITH ATTRACTIVE INTERACTION

In this paper, we consider the Hamiltonian of the correlated Chern insulator - spinful Haldane model on honeycomb lattice with the on-site attractive interaction as[8-11]

$$H = H_H + H' - U \sum_i \hat{n}_{i\uparrow} \hat{n}_{i\downarrow} - \mu \sum_{\langle i, \sigma \rangle} \hat{c}_{i\sigma}^\dagger \hat{c}_{i\sigma}. \quad (1)$$

where  $U > 0$  is the on-site interaction strength.  $\hat{n}_{i\uparrow}$  and  $\hat{n}_{i\downarrow}$  are the number operators of electrons with up-spin and that with down-spin, respectively.  $\sigma$  are the spin-indices representing spin-up ( $\sigma = \uparrow$ ) and spin-down ( $\sigma = \downarrow$ ) for electrons.  $\mu$  is the chemical potential and we only consider half-filling case by setting  $\mu = 0$ .  $H_H$  is the Hamiltonian of the spinful Haldane model which is given by

$$H_H = -t \sum_{\langle i, j \rangle, \sigma} \left( \hat{c}_{i\sigma}^\dagger \hat{c}_{j\sigma} + h.c. \right) - t' \sum_{\langle\langle i, j \rangle\rangle, \sigma} e^{i\phi_{ij}} \hat{c}_{i\sigma}^\dagger \hat{c}_{j\sigma} + h.c.$$

Here  $t$  and  $t'$  are the nearest neighbor and the next nearest neighbor, respectively. To break time-reversal symmetry, we introduce a complex phase  $\phi_{ij}$  into the second-neighbor hopping, and set the direction of the positive

\*Corresponding author; Electronic address: spkou@bnu.edu.cn

phase is clockwise ( $|\phi_{ij}| = \frac{\pi}{2}$ ).  $H'$  denotes an on-site staggered energy which is

$$H' = \varepsilon \sum_{i \in A, \sigma} \hat{c}_{i\sigma}^\dagger \hat{c}_{i\sigma} - \varepsilon \sum_{i \in B, \sigma} \hat{c}_{i\sigma}^\dagger \hat{c}_{i\sigma}.$$

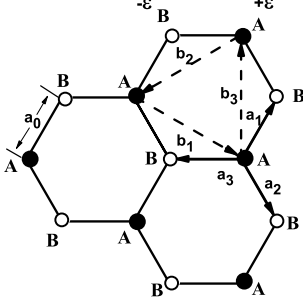


FIG. 1: (Color online) The illustration of the honeycomb lattice

Using the Fourier transformations, the electronic annihilation operators on the two sublattices are written into

$$\begin{aligned} \hat{c}_{i \in A, \sigma} &= \frac{1}{\sqrt{N_s}} \sum_{\mathbf{k}} e^{i\mathbf{k} \cdot \mathbf{R}_i} \hat{a}_{\mathbf{k}\sigma}, \\ \hat{c}_{i \in B, \sigma} &= \frac{1}{\sqrt{N_s}} \sum_{\mathbf{k}} e^{i\mathbf{k} \cdot \mathbf{R}_i} \hat{b}_{\mathbf{k}\sigma}. \end{aligned} \quad (2)$$

$N_s$  denotes the number of unit cells. For free fermions (the on-site Coulomb repulsion  $U$  is zero), the spectrum is

$$\mathbf{E}_{\mathbf{k}} = \pm \sqrt{|\xi_{\mathbf{k}}|^2 + (\gamma_{\mathbf{k}} + \varepsilon)^2} \quad (3)$$

where

$$\begin{aligned} |\xi_{\mathbf{k}}| &= \left| t \sum_{i=1}^3 e^{i\mathbf{k} \cdot \mathbf{a}_i} \right| \\ &= t \sqrt{3 + 2 \cos(\sqrt{3}k_y) + 4 \cos(3k_x/2) \cos(\sqrt{3}k_y/2)} \end{aligned} \quad (4)$$

and

$$\gamma_{\mathbf{k}} = 2t' \sum_i \sin(\mathbf{k} \cdot \mathbf{b}_i).$$

The parameters  $\mathbf{a}_1, \mathbf{a}_2$  and  $\mathbf{a}_3$  are the nearest neighbors of the A sublattice (See Fig.1) which are defined as

$$\mathbf{a}_1 = a_0 \left( \frac{1}{2}, \frac{\sqrt{3}}{2} \right), \mathbf{a}_2 = a_0 \left( \frac{1}{2}, -\frac{\sqrt{3}}{2} \right), \mathbf{a}_3 = a_0 (-1, 0) \quad (5)$$

and  $\mathbf{b}_1 = \mathbf{a}_2 - \mathbf{a}_3, \mathbf{b}_2 = \mathbf{a}_3 - \mathbf{a}_1, \mathbf{b}_3 = \mathbf{a}_1 - \mathbf{a}_2$ .  $a_0$  is the length of the hexagon side and is set to be unit.

From the spectrum of free fermions, we can see that there exist energy gaps near the points  $\mathbf{k}_1 = \frac{2\pi}{3}(1, \frac{1}{\sqrt{3}})$  and  $\mathbf{k}_2 = -\frac{2\pi}{3}(1, \frac{1}{\sqrt{3}})$  as

$$\Delta E = \left| 2\varepsilon - 6\sqrt{3}t' \right|$$

When the energy gap closed, we can get the phase boundary. We can see that there exist two phases in the free electron case: the topological insulator with anomalous quantum Hall effect (we call it QAH) and the normal band insulator (NI) state. For each spin-component of fermions, the Chern number is defined by

$$C = \frac{1}{4\pi} \int_{\Omega} d^2k [\mathbf{n} \cdot \partial_x \mathbf{n} \times \partial_y \mathbf{n}] = \pm 1 \quad (6)$$

where  $\mathbf{n}$  is defined as  $\mathbf{n} = \frac{\mathbf{d}}{|\mathbf{d}|}$  where

$$\mathbf{d} = (d_x, d_y, d_z)$$

and

$$\begin{aligned} d_x &= \text{Re } \xi_{\mathbf{k}}, \\ d_y &= \text{Im } \xi_{\mathbf{k}}, \\ d_z &= \gamma_{\mathbf{k}} + \varepsilon. \end{aligned}$$

Then at zero temperature ( $T = 0$ ), due to spin rotation symmetry, we obtain  $C = \pm 2$  in QAH and  $C = 0$  in NI. The eigen-state of the two states are depicted in Fig.2 and Fig.3. One can see that there is gapless edge states in QAH while no edge states in NI.

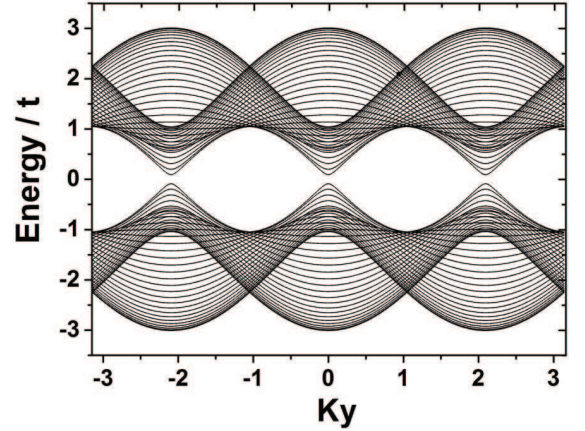


FIG. 2: (Color online) The edge states of normal insulator with open armchair boundary. The parameters are  $t'/t = 0.05$ ,  $\varepsilon/t = 0.3$ .

### III. MEAN FIELD PHASE DIAGRAM AND TOPOLOGICAL QUANTUM PHASE TRANSITION

When increasing the interaction strength, we get an  $s$ -wave pairing SC order. The SC order parameter of the

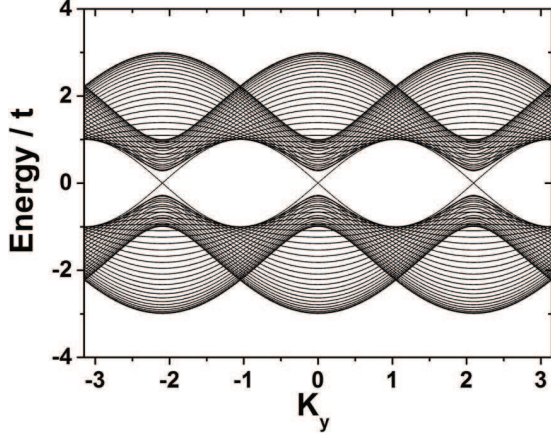


FIG. 3: (Color online) The edge states of topological insulator (or QAH) with open armchair boundary. The parameters are  $t'/t = 0.05$ ,  $\varepsilon/t = 0.01$ .

$s$ -wave SC is

$$\langle \hat{c}_{i,\uparrow}^\dagger \hat{c}_{i,\downarrow}^\dagger \rangle = \Delta.$$

Then in the mean field approach, the Hamiltonian can be written as

$$H = H_H + H' - U\Delta \sum_i \hat{c}_{i,\uparrow}^\dagger \hat{c}_{i,\downarrow}^\dagger + h.c.. \quad (7)$$

In the momentum space, it becomes

$$H = \sum_k \Psi_k^\dagger h_k \Psi_k \quad (8)$$

where the basis vector  $\Psi_k^\dagger$  is  $(\hat{a}_{\mathbf{k}\uparrow}^\dagger \ \hat{a}_{-\mathbf{k}\downarrow} \ \hat{b}_{\mathbf{k}\uparrow}^\dagger \ \hat{b}_{-\mathbf{k}\downarrow})$  and

$$h_k = \begin{pmatrix} \gamma_k + \varepsilon & -U\Delta & -\xi_{\mathbf{k}} & 0 \\ -U\Delta & \gamma_k - \varepsilon & 0 & \xi_{\mathbf{k}} \\ -\xi_{\mathbf{k}}^* & 0 & -\gamma_k - \varepsilon & -U\Delta \\ 0 & \xi_{\mathbf{k}}^* & -U\Delta & -\gamma_k + \varepsilon \end{pmatrix}. \quad (9)$$

After diagonalization, we can obtain the spectrum of the quasi-particles

$$\mathbf{E}_{\mathbf{k}_1} = \pm \sqrt{(|\gamma_k| + \sqrt{(U\Delta)^2 + \varepsilon^2})^2 + |\xi_k|^2} \quad (10)$$

and

$$\mathbf{E}_{\mathbf{k}_2} = \pm \sqrt{(|\gamma_k| - \sqrt{(U\Delta)^2 + \varepsilon^2})^2 + |\xi_k|^2}. \quad (11)$$

Then in mean field approach, we get the self-consistency equation to derive  $\Delta$  by minimizing the en-

ergy in the reduced Brillouin zone as

$$1 = \frac{1}{4N_s} \sum_{\mathbf{k}} \left[ \frac{(|\gamma_k| + \sqrt{(U\Delta)^2 + \varepsilon^2}) \frac{(U)}{\sqrt{(U\Delta)^2 + \varepsilon^2}}}{\sqrt{(|\gamma_k| + \sqrt{(U\Delta)^2 + \varepsilon^2})^2 + |\xi_k|^2}} - \frac{(|\gamma_k| - \sqrt{(U\Delta)^2 + \varepsilon^2}) \frac{(U)}{\sqrt{(U\Delta)^2 + \varepsilon^2}}}{\sqrt{(|\gamma_k| - \sqrt{(U\Delta)^2 + \varepsilon^2})^2 + |\xi_k|^2}} \right]. \quad (12)$$

To determine the phase diagram, there are four types of phase transitions : the quantum phase transition between topological  $s$ -wave SC order with  $\Delta \neq 0$  and QAH with  $\Delta = 0$ , the topological quantum phase transition between topological  $s$ -wave SC order with  $\Delta \neq 0$  and the normal  $s$ -wave SC state with  $\Delta \neq 0$ , the quantum phase transition between NI with  $\Delta = 0$  and QAH with  $\Delta = 0$ , the quantum phase transition between NI and the normal  $s$ -wave SC state with  $\Delta \neq 0$ . In particular, the topological quantum phase transition between TSC and normal  $s$ -wave SC is determined by the condition of zero quasi-particle's energy gap

$$\Delta_f = 2(3\sqrt{3}t' - \sqrt{(U\Delta)^2 + \varepsilon^2}) = 0. \quad (13)$$

After determining the phase boundaries, we plot the phase diagram in Fig.4. In the phase diagram of Fig.4, there exist four different quantum phases : QAH, NI,  $C = \pm 2$  topological  $s$ -wave SC and the normal  $s$ -wave SC.

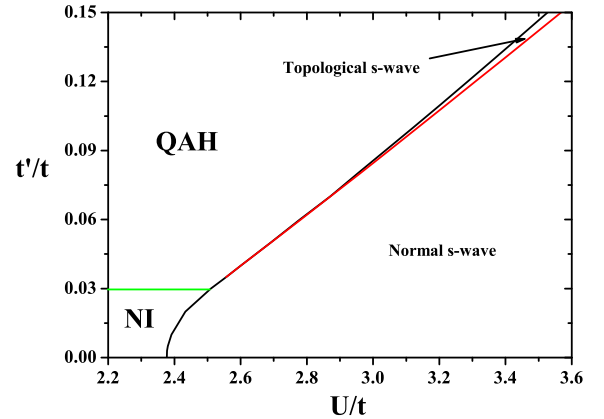


FIG. 4: (Color online) The phase diagram of the case  $\varepsilon/t = 0.15$  at  $T = 0$ . There exist four phases : the NI state, the QAH state, the topological  $s$ -wave state and the normal  $s$ -wave.

From Fig.4, one can see that in the non-interacting limit ( $U = 0$ ), the ground state is a  $C = \pm 2$  topological insulator with QAH for  $t' > 0.0288t$  and NI for  $t' < 0.0288t$ . At  $t' = 0.0288t$ , the electron energy gap closes at high symmetry points in the momentum space.

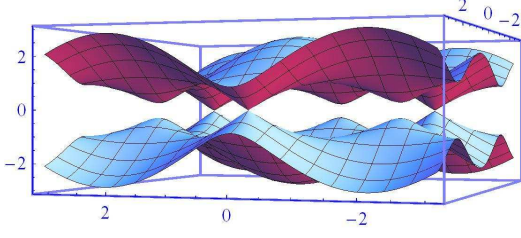


FIG. 5: (Color online) The dispersion of electrons for  $t' = 0.0288t$  when  $U = 0$ . We can see clearly that in the high symmetry point the energy gap is zero and the dispersion has a Dirac cone.

As a result, a third order topological quantum phase transition occurs between QAH and NI. See the dispersion of electrons for  $t' = 0.0288t$  in Fig.5. With the increasing of the on-site Coulomb interaction strength, the ground state can be an  $s$ -wave superconductor. For  $t' > 0.0288t$ , the quantum phase transition between QAH and  $s$ -wave order is always first order which is denoted by the black line in Fig.4.

In the region of  $0.0288t < t' < 0.035t$ , due to the jumping of the superconductor order, the QAH state will turn into normal  $s$ -wave state without gap closing. In Fig.6 and Fig.7, we plot the SC order parameter and the energy gap for the case of  $\varepsilon/t = 0.15$ ,  $t'/t = 0.03$ . While in the region of  $t' > 0.035t$ , with the increasing of the interaction strength  $U$ , due to the smoothly change of the SC order parameter, the NI state will turn into the topological  $s$ -wave SC order after crossing a first order phase transition (black line in Fig.4) and then turn into the normal  $s$ -wave order crossing a second order quantum phase transition (red line in Fig.4). In Fig.8 and Fig.9, we also plot the SC order parameter and the energy gap for the case of  $\varepsilon/t = 0.15$ ,  $t'/t = 0.1$ . In the region of  $t' < 0.0288t$ , the quantum phase transition between NI and  $s$ -wave SC order is always second order which is denoted by the black line in Fig.4. With the increase of the interaction strength  $U$ , due to the smoothly change of the SC order parameter, the NI state will turn into the normal  $s$ -wave order after crossing a second order phase transition. In Fig.10, we plot the SC order parameter for the case of  $\varepsilon/t = 0.15$ ,  $t'/t = 0.01$ .

#### IV. TOPOLOGICAL PROPERTIES OF TSC

In this section we will study the topological properties in the TSC state. The  $s$ -wave paired ground state exhibits a non-trivial topological property that can be signified by the Chern number  $C = \pm 2$  in the momentum space. Because the pairing is  $s$ -wave, such TSC be-

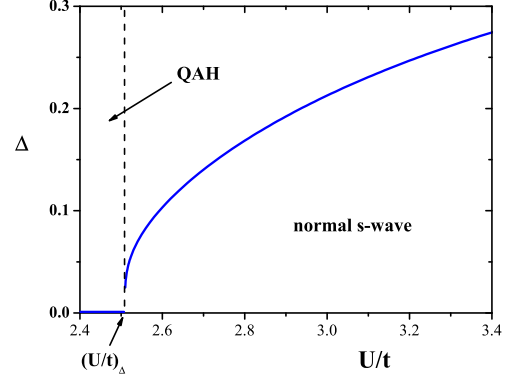


FIG. 6: (Color online) The superconductor order  $\Delta$  for the case of  $\varepsilon/t = 0.15$  and  $t'/t = 0.03$ .  $(\frac{U}{t})_\Delta$  is the critical point of the superconductor order phase transition.

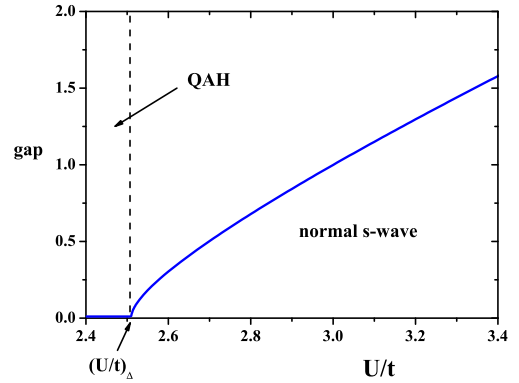


FIG. 7: (Color online) The energy gap  $\Delta_f$  for the case of  $\varepsilon/t = 0.15$  and  $t'/t = 0.03$ .  $(\frac{U}{t})_\Delta$  is the critical point of the superconductor order phase transition.

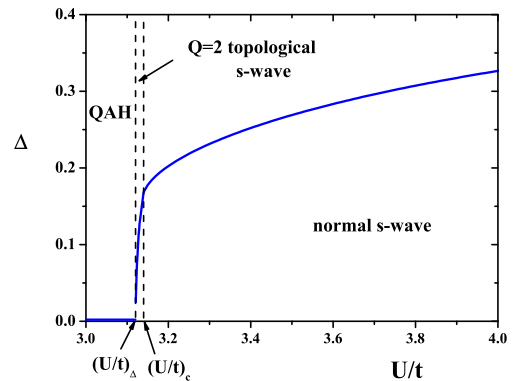


FIG. 8: (Color online) The superconductor order  $\Delta$  for the case of  $\varepsilon/t = 0.15$  and  $t'/t = 0.1$ .  $(\frac{U}{t})_\Delta$  is the critical point of the superconductor order phase transition and  $(\frac{U}{t})_c$  is the topological quantum phase transition.



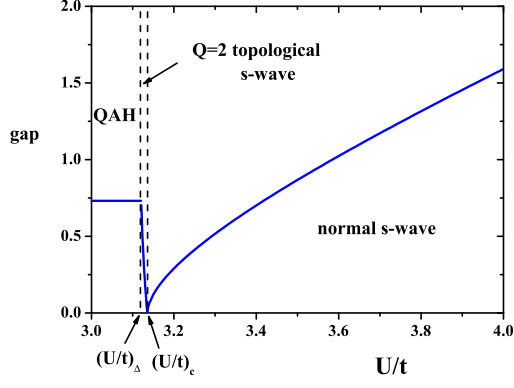


FIG. 9: (Color online) The energy gap  $\Delta_f$  for the case of  $\varepsilon/t = 0.15$  and  $t'/t = 0.1$ .  $(\frac{U}{t})_\Delta$  is the critical point of the superconductor order phase transition and  $(\frac{U}{t})_c$  is the topological quantum phase transition.

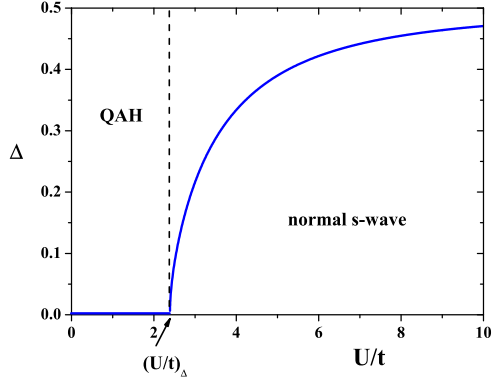


FIG. 10: (Color online) The superconductor order  $\Delta$  for the case of  $\varepsilon/t = 0.15$  and  $t'/t = 0.01$ .  $(\frac{U}{t})_\Delta$  is the critical point of the superconductor order phase transition.

longs to topological superconductor. In this section we calculate the edge states and the zero modes around the  $\pi$ -flux.

### A. Edge states

In this part, we study the edge states of TSC. The dispersion of the edge states of normal SC and that of TSC are plotted in Fig.11 and Fig.12, respectively. From them, we find there exist no gapless edge states in the normal SC. While for TSC there always exist two gapless edge states.

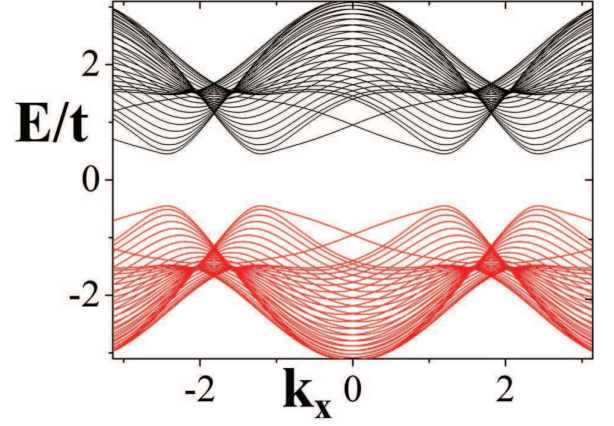


FIG. 11: (Color online) The edge states of normal SC with "zigzag" open boundary for parameters  $t'/t = 0.1$ ,  $\varepsilon/t = 0.15$ ,  $U/t = 3.5$ .

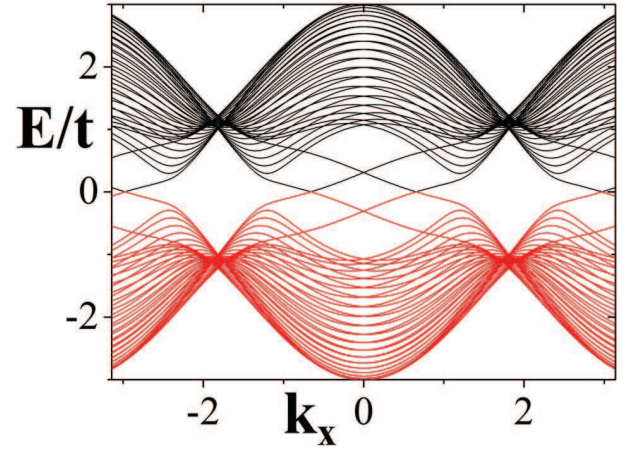


FIG. 12: (Color online) The edge states of TSC with "zigzag" open boundary for parameters  $t'/t = 0.1$ ,  $\varepsilon/t = 0.15$ ,  $U/t = 3.125$ .

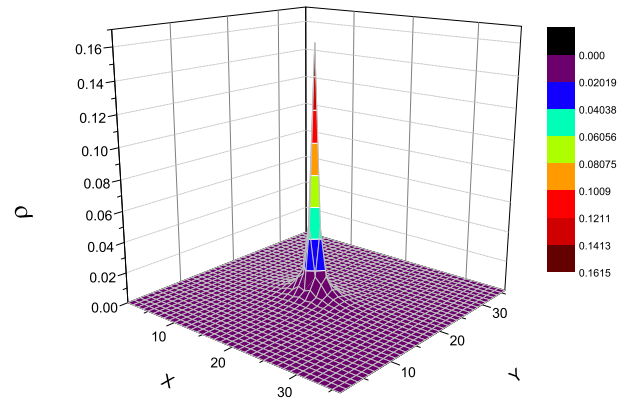


FIG. 13: (Color online) The particle density around a  $\pi$ -flux in TSC.

### B. Zero modes of $\pi$ -flux

After recognizing the properties of edge states, we turn to study  $\pi$ -flux. A  $\pi$ -flux denotes half a flux quantum one plaquette of the square lattice,  $\frac{1}{2}\Phi_0$  ( $\Phi_0 = \frac{h\epsilon}{e}$ ). For a TSC on a honeycomb lattice, a  $\pi$ -flux on a plaquette is confined at zero temperature and cannot be real excitation. From the numerical calculations, we found that there exist two zero modes around each  $\pi$ -flux. And in Fig.13, we plot the particle density around a  $\pi$ -flux in TSC phase.

### V. PHASE STIFFNESS

In this section we study the phase fluctuations of TSC going beyond mean field method by random-phase-approximation (RPA) approach [13]. Now the SC order parameters become  $\Delta(i) = |\Delta|e^{i\theta_i}$ . For the fluctuated SC order parameters  $\Delta(i)$ , there are two bosonic modes : a gapped amplitude mode and the Goldstone mode (the mode describing phase fluctuations).

In the imaginary-time path-integral representation ( $\beta = 1/T$ ,  $\hbar = k_B = 1$ ), using the Hubbard-Stratonovich transformation, the partition function can be written as[12]

$$Z = \int [dc_\sigma^* dc_\sigma] [d\Delta^* d\Delta] e^{-S(c_\sigma^*, c_\sigma, \Delta^*, \Delta)} \quad (14)$$

$$S = \int_0^\beta d\tau \sum_{\mathbf{r}} \left\{ \frac{1}{U} \Delta^* \Delta + c_\sigma^* \partial_\tau c_\sigma^* + H_t + H_{t'} + H_\varepsilon - \Delta(\mathbf{r}, \tau) c_\sigma(\mathbf{r}, \tau) c_{\bar{\sigma}}(\mathbf{r}, \tau) - \Delta^*(\mathbf{r}, \tau) c_{\bar{\sigma}}^*(\mathbf{r}, \tau) c_\sigma^*(\mathbf{r}, \tau) \right\}.$$

After integrating over the electron fields, in the momentum space, the action can be written as

$$S = \frac{\beta}{U} \sum_{q, \eta=A, B} \Delta_\eta^*(q) \Delta_\eta(q) + 2\beta\mu N - \sum_q \ln G^{-1}$$

where  $\Delta_\eta(q) = \Delta_{\eta,0} + \Lambda_\eta(q)$ ,  $\Delta_{\eta,0} = \Delta_0$  and  $G^{-1} = G_0^{-1} + G_1^{-1}$  with

$$G_0^{-1} = \begin{pmatrix} i\omega_m + \gamma_{\mathbf{k}} + \varepsilon & -\Delta_0 & -\xi_k & 0 \\ -\Delta_0 & i\omega_m + \gamma_{\mathbf{k}} - \varepsilon & 0 & \xi_k \\ -\xi_k^* & 0 & i\omega_m - \gamma_{\mathbf{k}} - \varepsilon & -\Delta_0 \\ 0 & \xi_k^* & -\Delta_0 & i\omega_m - \gamma_{\mathbf{k}} + \varepsilon \end{pmatrix}$$

and

$$G_1^{-1} = \begin{pmatrix} 0 & -\Lambda_A(q) & 0 & 0 \\ -\Lambda_A^*(-q) & 0 & 0 & 0 \\ 0 & 0 & 0 & -\Lambda_B(q) \\ 0 & 0 & -\Lambda_B^*(-q) & 0 \end{pmatrix}. \quad (15)$$

Here we have used

$$\begin{aligned} \Lambda_\eta(q) &= \frac{1}{\sqrt{N}} \int dx \Lambda_\eta(x) e^{-iq \cdot x} \\ \Lambda_\eta^*(-q) &= \frac{1}{\sqrt{N}} \int dx \Lambda_\eta^*(x) e^{-iq \cdot x} \\ \Lambda_\eta(x) &= \frac{1}{\sqrt{N}} \sum_q \Lambda_\eta(q) e^{iq \cdot x} \\ \Lambda_\eta^*(x) &= \frac{1}{\sqrt{N}} \sum_q \Lambda_\eta^*(q) e^{-iq \cdot x} \end{aligned}$$

Next, we investigate the Gaussian fluctuations around the saddle point. Using the expansion of the natural logarithm of

$$\begin{aligned} \text{Tr} \ln G^{-1} &= \ln(G_0^{-1} + G_1^{-1}) \\ &= \text{Tr} \ln G_0^{-1} - \sum_{l=1}^{\infty} \frac{(-1)^l}{l} \text{Tr}(G_0 G_1^{-1})^l, \end{aligned} \quad (16)$$

we expand the action to second order of the fluctuation fields  $\Lambda_\eta(q)$ . This procedure leads to an effective action as

$$S = S_0 + S'_1 \quad (17)$$

where the effective action at the saddle point is

$$S_0 = \frac{\beta}{U} \sum_{\eta=A, B} \Delta_{\eta,0} \Delta_{\eta,0} + 2\beta\mu N - \text{Tr} \ln G_0^{-1} \quad (18)$$

and the effective action corresponding the quantum fluctuations reads

$$\begin{aligned} S'_1 &= \frac{1}{2} \text{Tr} \sum_{q, p} (G_0(p) G_1^{-1}(p, p-q) G_0(p-q) G_1^{-1}(p-q, p)) \\ &\quad + \frac{\beta}{U} \sum_{q, \eta=A, B} \Delta_\eta^*(q) \Delta_\eta(q) \\ &= S_1 + S_2 \end{aligned} \quad (19)$$

where

$$S_2 = \frac{\beta}{U} \sum_{q, \eta=A, B} \Delta_\eta^*(q) \Delta_\eta(q) \quad (20)$$

and

$$S_1 = \frac{\beta}{2} \sum_q \Lambda_q^\dagger Q'(q) \Lambda_q. \quad (21)$$

Here  $\Lambda_q^\dagger = (\Lambda_A^*(-q), \Lambda_A(q), \Lambda_B(q), \Lambda_B^*(-q))$  denotes the fluctuation field and  $Q'(q)$  is given by the following matrix

$$Q'(q) = \begin{pmatrix} Q'_{11}(q) & Q'_{12}(q) & Q'_{13}(q) & Q'_{14}(q) \\ Q'_{21}(q) & Q'_{22}(q) & Q'_{23}(q) & Q'_{24}(q) \\ Q'_{31}(q) & Q'_{32}(q) & Q'_{33}(q) & Q'_{34}(q) \\ Q'_{41}(q) & Q'_{42}(q) & Q'_{43}(q) & Q'_{44}(q) \end{pmatrix} \quad (22)$$

where

$$\begin{aligned} Q'_{11}(q) &= \frac{1}{\beta N} \sum_p G_{022}(p) G_{011}(p-q), \\ Q'_{12}(q) &= \frac{1}{\beta N} \sum_p G_{012}(p) G_{012}(p-q), \\ Q'_{13}(q) &= \frac{1}{\beta N} \sum_p G_{032}(p) G_{014}(p-q), \\ Q'_{14}(q) &= \frac{1}{\beta N} \sum_p G_{042}(p) G_{013}(p-q), \quad (23) \\ Q'_{21}(q) &= \frac{1}{\beta N} \sum_p G_{021}(p) G_{021}(p-q), \\ Q'_{22}(q) &= \frac{1}{\beta N} \sum_p G_{011}(p) G_{022}(p-q), \\ Q'_{23}(q) &= \frac{1}{\beta N} \sum_p G_{031}(p) G_{024}(p-q), \\ Q'_{24}(q) &= \frac{1}{\beta N} \sum_p G_{041}(p) G_{023}(p-q), \quad (24) \end{aligned}$$

$$\begin{aligned} Q'_{31}(q) &= \frac{1}{\beta N} \sum_p G_{023}(p) G_{041}(p-q), \\ Q'_{32}(q) &= \frac{1}{\beta N} \sum_p G_{013}(p) G_{042}(p-q), \\ Q'_{33}(q) &= \frac{1}{\beta N} \sum_p G_{033}(p) G_{044}(p-q), \\ Q'_{34}(q) &= \frac{1}{\beta N} \sum_p G_{043}(p) G_{043}(p-q), \quad (25) \end{aligned}$$

$$\begin{aligned} Q'_{41}(q) &= \frac{1}{\beta N} \sum_p G_{024}(p) G_{031}(p-q), \\ Q'_{42}(q) &= \frac{1}{\beta N} \sum_p G_{014}(p) G_{032}(p-q), \\ Q'_{43}(q) &= \frac{1}{\beta N} \sum_p G_{034}(p) G_{034}(p-q), \\ Q'_{44}(q) &= \frac{1}{\beta N} \sum_p G_{044}(p) G_{033}(p-q). \quad (26) \end{aligned}$$

See the details of  $G_0$  in appendix.

For the term  $Q'_{ij}(q)$ , using the Matsubara summation formula as  $1/\beta \sum_{\omega_m} 1/(i\omega_m - E) = n_F(E)$ , at zero temperature we may obtain

$$\begin{aligned}
Q'_{ij}(q) &= \frac{1}{\beta N} \sum_p G_{0kl}(p) G_{0mn}(p-q) \\
&= \frac{1}{N} \sum_{\mathbf{k}} \frac{1}{\beta} \sum_{\omega_m} \left( \frac{A_{kl}}{i\omega_m + E_+(\mathbf{k})} + \frac{B_{kl}}{i\omega_m - E_+(\mathbf{k})} + \right. \\
&\quad \left. \frac{C_{kl}}{i\omega_m + E_-(\mathbf{k})} + \frac{D_{kl}}{i\omega_m - E_-(\mathbf{k})} \right) \left( \frac{A_{mn}}{i\omega_m - i\omega_n + E_+(\mathbf{k}-\mathbf{q})} \right. \\
&\quad \left. + \frac{B_{mn}}{i\omega_m - i\omega_n - E_+(\mathbf{k}-\mathbf{q})} + \frac{C_{mn}}{i\omega_m - i\omega_n + E_-(\mathbf{k}-\mathbf{q})} \right. \\
&\quad \left. + \frac{D_{mn}}{i\omega_m - i\omega_n - E_-(\mathbf{k}-\mathbf{q})} \right) \\
&= \frac{1}{N} \left[ \sum_{\mathbf{k}} \frac{A_{kl} B_{mn}}{-i\omega_n - E_+(\mathbf{k}-\mathbf{q}) - E_+(\mathbf{k})} + \sum_{\mathbf{k}} \frac{A_{kl} D_{mn}}{-i\omega_n - E_-(\mathbf{k}-\mathbf{q}) - E_+(\mathbf{k})} \right. \\
&\quad \left. \sum_{\mathbf{k}} \frac{-B_{kl} A_{mn}}{-i\omega_n + E_+(\mathbf{k}-\mathbf{q}) + E_+(\mathbf{k})} + \sum_{\mathbf{k}} \frac{-B_{kl} C_{mn}}{-i\omega_n + E_-(\mathbf{k}-\mathbf{q}) + E_+(\mathbf{k})} \right. \\
&\quad \left. \sum_{\mathbf{k}} \frac{C_{kl} B_{mn}}{-i\omega_n - E_+(\mathbf{k}-\mathbf{q}) - E_-(\mathbf{k})} + \sum_{\mathbf{k}} \frac{C_{kl} D_{mn}}{-i\omega_n - E_-(\mathbf{k}-\mathbf{q}) - E_-(\mathbf{k})} \right. \\
&\quad \left. \sum_{\mathbf{k}} \frac{-D_{kl} A_{mn}}{-i\omega_n + E_+(\mathbf{k}-\mathbf{q}) + E_-(\mathbf{k})} + \sum_{\mathbf{k}} \frac{D_{kl} C_{mn}}{-i\omega_n + E_-(\mathbf{k}-\mathbf{q}) + E_-(\mathbf{k})} \right]
\end{aligned}$$


---

where  $\omega_m = (2n+1)\pi/\beta$ ,  $\omega_n = 2n\pi/\beta$ , and  $n_F(E)$  is the Fermi distribution function which reads  $n_F(E) = 1/(e^{\beta E} + 1)$ . When the usual analytic continuation  $i\omega_n \rightarrow \omega + i0^+$  is performed, and in static limit  $\omega = 0$ ,  $Q'_{ij}(q)$  is reduced into

$$\begin{aligned}
Q'_{ij}(q) &= \frac{-1}{N} \left[ \sum_{\mathbf{k}} \frac{A_{kl}(\mathbf{k}) B_{mn}(\mathbf{k}-\mathbf{q}) + B_{kl}(\mathbf{k}) A_{mn}(\mathbf{k}-\mathbf{q})}{E_+(\mathbf{k}-\mathbf{q}) + E_+(\mathbf{k})} \right. \\
&\quad + \sum_{\mathbf{k}} \frac{A_{kl}(\mathbf{k}) D_{mn}(\mathbf{k}-\mathbf{q}) + B_{kl}(\mathbf{k}) C_{mn}(\mathbf{k}-\mathbf{q})}{E_-(\mathbf{k}-\mathbf{q}) + E_+(\mathbf{k})} + \\
&\quad \sum_{\mathbf{k}} \frac{C_{kl}(\mathbf{k}) B_{mn}(\mathbf{k}-\mathbf{q}) + D_{kl}(\mathbf{k}) A_{mn}(\mathbf{k}-\mathbf{q})}{E_+(\mathbf{k}-\mathbf{q}) + E_-(\mathbf{k})} + \\
&\quad \left. \sum_{\mathbf{k}} \frac{C_{kl}(\mathbf{k}) D_{mn}(\mathbf{k}-\mathbf{q}) + D_{kl}(\mathbf{k}) C_{mn}(\mathbf{k}-\mathbf{q})}{E_-(\mathbf{k}-\mathbf{q}) + E_-(\mathbf{k})} \right]. \tag{27}
\end{aligned}$$

In order to obtain the phase stiffness, we can express  $\Lambda_\eta(q) = \chi_\eta(q) e^{i\varphi_\eta(q)} = [\lambda_\eta(q) + i\theta_\eta(q)]/\sqrt{2}$ , where  $\chi_\eta(q)$ ,  $\varphi_\eta(q)$ ,  $\lambda_\eta(q)$  and  $\theta_\eta(q)$  are the real fields.  $\lambda_\eta(q)$  and  $\theta_\eta(q)$  essentially can be regarded as the amplitude field and the phase field, respectively. For the general cases,  $\varphi_\eta(q)$  is

small[13]. Then the field  $\Lambda_q$  in the new basis  $\begin{pmatrix} \lambda_A(q) \\ \theta_A(q) \\ \theta_B(q) \\ \lambda_B(q) \end{pmatrix}$

is given by

$$\Lambda_q = \frac{1}{\sqrt{2}} \begin{pmatrix} 1 & i & 0 & 0 \\ 1 & -i & 0 & 0 \\ 0 & 0 & -i & 1 \\ 0 & 0 & i & 1 \end{pmatrix}. \tag{28}$$

In a rotated basis, the matrix  $Q'(q)$  can be changed into  $\tilde{Q}(q)$ . Now we have the action of the quantum fluctuations as

$$S_1 = \frac{\beta}{2} \sum_q \Phi_q^\dagger \tilde{Q}(q) \Phi_q \tag{29}$$

where  $\Phi_q^\dagger = (\lambda_A(q), \theta_A(q), \theta_B(q), \lambda_B(q))$  and  $\tilde{Q}(q)$  in this



rotated basis reads

$$\begin{aligned}
\tilde{Q}_{11}(q) &= (Q'_{11} + Q'_{21} + Q'_{12} + Q'_{22})/2, \\
\tilde{Q}_{12}(q) &= (iQ'_{11} + iQ'_{21} - iQ'_{12} - iQ'_{22})/2, \\
\tilde{Q}_{13}(q) &= (-iQ'_{13} - iQ'_{23} + iQ'_{14} + iQ'_{24})/2, \\
\tilde{Q}_{14}(q) &= (Q'_{13} + Q'_{23} + Q'_{14} + Q'_{24})/2, \\
\tilde{Q}_{21}(q) &= (-iQ'_{11} + iQ'_{21} - iQ'_{12} + iQ'_{22})/2, \\
\tilde{Q}_{22}(q) &= (Q'_{11} - Q'_{21} - Q'_{12} + Q'_{22})/2, \\
\tilde{Q}_{23}(q) &= (-Q'_{13} + Q'_{23} + Q'_{14} - Q'_{24})/2, \\
\tilde{Q}_{24}(q) &= (-iQ'_{13} + iQ'_{23} - iQ'_{14} + iQ'_{24})/2, \\
\tilde{Q}_{31}(q) &= (iQ'_{31} - iQ'_{41} + iQ'_{32} - iQ'_{42})/2, \\
\tilde{Q}_{32}(q) &= (-Q'_{31} + Q'_{41} + Q'_{32} - Q'_{42})/2, \\
\tilde{Q}_{33}(q) &= (Q'_{33} - Q'_{43} - Q'_{34} + Q'_{44})/2, \\
\tilde{Q}_{34}(q) &= (iQ'_{33} - iQ'_{43} + iQ'_{34} - iQ'_{44})/2, \\
\tilde{Q}_{41}(q) &= (Q'_{31} + Q'_{41} + Q'_{32} + Q'_{42})/2, \\
\tilde{Q}_{42}(q) &= (iQ'_{31} + iQ'_{41} - iQ'_{32} - iQ'_{42})/2, \\
\tilde{Q}_{43}(q) &= (-iQ'_{33} - iQ'_{43} + iQ'_{34} + iQ'_{44})/2, \\
\tilde{Q}_{44}(q) &= (Q'_{33} + Q'_{43} + Q'_{34} + Q'_{44})/2.
\end{aligned} \tag{30}$$

Next, we focus on the phase fluctuations. Upon integration of the amplitude fields we obtain a phase-only effective action as

$$S_1 = \frac{\beta}{2} \sum_q \theta^\dagger(q) \tilde{Q}_{phase}(q) \theta(q), \tag{31}$$

where  $\theta^\dagger(q) = (\theta_A(q), \theta_B(q))$ . The matrix  $\tilde{Q}_{phase}$  corresponding to phase-phase fluctuation is given by

$$\tilde{Q}_{phase}(q) = \begin{pmatrix} \tilde{Q}_{ph11} & \tilde{Q}_{ph12} \\ \tilde{Q}_{ph21} & \tilde{Q}_{ph22} \end{pmatrix} \tag{32}$$

where

$$\begin{aligned}
\tilde{Q}_{ph11} &= -(\tilde{Q}_{21}M'_{11}\tilde{Q}_{12} + \tilde{Q}_{24}M'_{21}\tilde{Q}_{12} + \tilde{Q}_{21}M'_{12}\tilde{Q}_{42} + \tilde{Q}_{24}M'_{22}\tilde{Q}_{42}) + \tilde{Q}_{22} \\
\tilde{Q}_{ph12} &= -(\tilde{Q}_{21}M'_{11}\tilde{Q}_{13} + \tilde{Q}_{24}M'_{21}\tilde{Q}_{13} + \tilde{Q}_{21}M'_{12}\tilde{Q}_{43} + \tilde{Q}_{24}M'_{22}\tilde{Q}_{43}) + \tilde{Q}_{23} \\
\tilde{Q}_{ph21} &= -(\tilde{Q}_{31}M'_{11}\tilde{Q}_{12} + \tilde{Q}_{34}M'_{21}\tilde{Q}_{12} + \tilde{Q}_{31}M'_{12}\tilde{Q}_{42} + \tilde{Q}_{34}M'_{22}\tilde{Q}_{42}) + \tilde{Q}_{32} \\
\tilde{Q}_{ph22} &= -(\tilde{Q}_{31}M'_{11}\tilde{Q}_{13} + \tilde{Q}_{34}M'_{21}\tilde{Q}_{13} + \tilde{Q}_{31}M'_{12}\tilde{Q}_{43} + \tilde{Q}_{34}M'_{22}\tilde{Q}_{43}) + \tilde{Q}_{33}
\end{aligned}$$

with the matrix  $M'(q)$

$$M'(q) = \begin{pmatrix} \frac{\tilde{Q}_{44}(q)}{Z(q)} & \frac{-\tilde{Q}_{14}(q)}{Z(q)} \\ \frac{-\tilde{Q}_{41}(q)}{Z(q)} & \frac{\tilde{Q}_{11}(q)}{Z(q)} \end{pmatrix} \tag{33}$$

where

$$Z(q) = \tilde{Q}_{11}(q)\tilde{Q}_{44}(q) - \tilde{Q}_{14}(q)\tilde{Q}_{41}(q). \tag{34}$$

Finally, the total phase-only effective action becomes

$$S'_1 = \beta/2 \sum_q \theta^\dagger(q) \tilde{Q}'_{phase}(q) \theta(q) \tag{35}$$

where the matrix  $\tilde{Q}'_{phase}(q)$  reads as

$$\begin{aligned}
\tilde{Q}'_{phase}(q) &= \begin{pmatrix} \frac{1}{U} + \tilde{Q}_{ph11} & \tilde{Q}_{ph12} \\ \tilde{Q}_{ph21} & \frac{1}{U} + \tilde{Q}_{ph22} \end{pmatrix} \\
&= \begin{pmatrix} \tilde{Q}'_{ph11} & \tilde{Q}'_{ph12} \\ \tilde{Q}'_{ph21} & \tilde{Q}'_{ph22} \end{pmatrix}.
\end{aligned} \tag{36}$$

The zero temperature superfluid density (phase stiffness)  $\rho_s(0)$  is obtained by examining the Goldstone mode action in the static limit. We numerically extract the zero temperature superfluid stiffness  $\rho_s(0)$  by identifying

$$\sqrt{\tilde{Q}'_{ph11}\tilde{Q}'_{ph22}} - \sqrt{\tilde{Q}'_{ph12}\tilde{Q}'_{ph21}} = [\sqrt{3}\rho_s(0)/2]\mathbf{q}^2 \tag{37}$$

for  $|\mathbf{q}| \rightarrow 0$  [14].

Now we derive the superfluid density (the phase stiffness) for the TSC at zero temperature  $\rho_s(0) = Q$ . After obtaining the phase stiffness  $\rho_s(0)$ , the effective Lagrangian of the phase fluctuations is given by

$$L_{\text{eff}} \simeq \frac{1}{2} \rho_s(0) (\nabla \theta)^2. \tag{38}$$

where  $\theta(x)$  denotes the phase fluctuations. See the results in Fig.15.

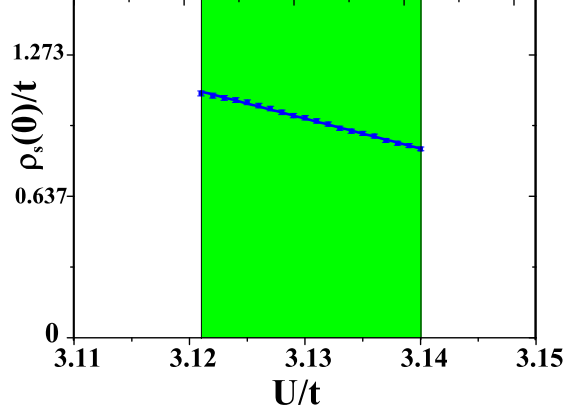


FIG. 14: (Color online) The phase stiffness of TSC order at  $T = 0$ . The green region is the TSC order.

## VI. PHYSICAL REALIZATION

In this end, we design an effective fermion model with  $C = \pm 2$  topological superfluid (SF) as its ground state in an optical lattice. When two-component fermions with repulsive interaction are put into a honeycomb optical lattice, one can get an effective interacting Haldane model. It is easy to change the potential barrier by varying the laser intensities to tune the Hamiltonian parameters including the hopping strength ( $t$ -term), the staggered potential ( $\varepsilon$ -term) and the particle interaction ( $U$ -term).

We first design an optical lattice of the Haldane model. The Haldane model had been proposed in the cold atoms with three blue detuned standing-wave lasers, of which the optical potential is given by  $V(x, y) = \sum_{j=1,2,3} V_0 \sin^2[k_L(x \cos \theta_j + y \sin \theta_j) + \pi/2]$  where  $V_0$  is the potential amplitude,  $\theta_1 = \pi/3$ ,  $\theta_2 = 2\pi/3$ ,  $\theta_3 = 0$ , and  $k_L$  is the optical wave vector in XY plane [15]. When two-component fermions are put into this honeycomb optical lattice, we may get an effective Haldane model by applying the Raman laser beams

$$\begin{aligned} \hat{H}_H = & -t \sum_{\langle i,j \rangle, \sigma} \hat{c}_{i,\sigma}^\dagger \hat{c}_{j,\sigma} - t' \sum_{\langle\langle i,j \rangle\rangle, \sigma} e^{i\phi_{ij}} \hat{c}_{i,\sigma}^\dagger \hat{c}_{j,\sigma} \\ & + \varepsilon \sum_{i \in A, \sigma} \hat{c}_{i\sigma}^\dagger \hat{c}_{i\sigma} - \varepsilon \sum_{i \in B, \sigma} \hat{c}_{i\sigma}^\dagger \hat{c}_{i\sigma} + h.c.. \end{aligned} \quad (39)$$

We introduce a complex phase  $\phi_{ij}$  ( $|\phi_{ij}| = \pi/2$ ) to the next nearest neighbor hopping, of which the positive phase is set to be clockwise. To design a complex phase of the next nearest neighbor hopping for two-component fermions generated by gauge field on the optical lattice, Raman laser beams in XY plane are applied with spacial-dependent Rabi frequencies as  $\Omega_0 \sin(\tilde{k}_L x + \frac{\pi}{4}) e^{iy\tilde{k}_L}$  and  $\Omega_0 \cos(\tilde{k}_L x + \frac{\pi}{4}) e^{-iy\tilde{k}_L}$  ( $\tilde{k}_L = 2\pi/(3a)$ ) where  $a$  denotes the length between nearest neighbor lattice sites. Then

we get a laser-field-generated effective gauge field on this honeycomb optical lattice as that given in Ref.[16].

In addition, we consider a strong interaction via Feshbach resonance technique  $\hat{H}_U = -U \sum_i \hat{n}_{i,\uparrow} \hat{n}_{i,\downarrow}$  where  $U > 0$  is the on-site attractive interaction strength [17, 18]. Thus, we may have an s-wave SF state by tuning the interaction between fermions via Feshbach resonance technique.

Finally we get an interacting two-component fermions system in 2D honeycomb optical lattice of the Haldane model as

$$\hat{H} = \hat{H}_H + \hat{H}_U - \mu \sum_{\langle i, \sigma \rangle} \hat{c}_{i\sigma}^\dagger \hat{c}_{i\sigma}. \quad (40)$$

where  $\mu$  denotes the chemical potential.

## VII. CONCLUSION

In this paper we studied the correlated Chern insulators by considering the electrons on the Haldane's model with on-site negative- $U$  interaction. We obtained its properties by using the mean field theory and RPA approach. We found that in the intermediate interaction region, the ground state becomes a TSC with the Chern number  $\pm 2$ . To characterize its topological properties, we studied its edge states and the zero modes on the  $\pi$ -flux. In the end we gave a proposal to realize such s-wave topological superconductor/superfluid by putting two-component (two pseudo-spins) interacting fermions on a honeycomb optical lattice.

## Acknowledgments

This work is supported by the National Basic Research Program of China (973 Program) under grant No. 2012CB921704, 2011CB921803, 2011cba00102 and NFSC Grant No. 11174035.

## VIII. APPENDIX: THE MATRIX $G_0$ OF RPA APPROACH TO DERIVE THE PHASE STIFFNESS OF TSC

In this appendix, we give the details about the matrix  $G_0 (= (G_0^{-1})^{-1})$  as

$$G_0 = \begin{pmatrix} G_{0,11} & G_{0,12} & G_{0,13} & G_{0,14} \\ G_{0,12} & G_{0,22} & G_{0,23} & G_{0,24} \\ G_{0,13}^* & G_{0,23}^* & G_{0,33} & G_{0,34} \\ G_{0,14}^* & G_{0,24}^* & G_{0,34} & G_{0,44} \end{pmatrix}. \quad (41)$$

Each element of  $G_0$  can be divided into

$$\begin{aligned}
 G_{0,ij} &= \frac{A_{ij}}{i\omega_m + E_+} + \frac{B_{ij}}{i\omega_m - E_+} \\
 &+ \frac{C_{ij}}{i\omega_m + E_-} + \frac{D_{ij}}{i\omega_m - E_-} \\
 &= \frac{\text{numerator}}{\text{denominator}}
 \end{aligned} \tag{42}$$

where the term "numerator" is

$$\begin{aligned}
 &-i\omega_m(A_{ij} + B_{ij} + C_{ij} + D_{ij})(\omega_m + |\xi_k|^2 + \Delta_0^2 + \varepsilon^2 + \gamma_k^2) \\
 &+ 2i\omega_m\gamma_k(A_{ij} + B_{ij} - C_{ij} - D_{ij})\sqrt{\Delta_0^2 + \varepsilon^2} \\
 &+ [(A_{ij} - B_{ij})E_+ + (C_{ij} - D_{ij})E_-](\omega_m + |\xi_k|^2 + \Delta_0^2 + \varepsilon^2 + \gamma_k^2) \\
 &+ [-(A_{ij} - B_{ij})E_+ + (C_{ij} - D_{ij})E_-]2\gamma_k\sqrt{\Delta_0^2 + \varepsilon^2}
 \end{aligned}$$

and the term "denominator" reads

$$(i\omega_m + E_+)(i\omega_m - E_+)(i\omega_m + E_-)(i\omega_m - E_-).$$

For the element  $G_{0,ij}$ , we can express the coefficients as

$$\begin{aligned}
 A_{ij} &= \frac{M_{ij} + N_{ij}}{4} + \frac{P_{ij} - Q_{ij}}{4E_+}, \\
 B_{ij} &= \frac{M_{ij} + N_{ij}}{4} - \frac{P_{ij} - Q_{ij}}{4E_+}, \\
 C_{ij} &= \frac{M_{ij} - N_{ij}}{4} + \frac{P_{ij} + Q_{ij}}{4E_-}, \\
 D_{ij} &= \frac{M_{ij} - N_{ij}}{4} - \frac{P_{ij} + Q_{ij}}{4E_-},
 \end{aligned} \tag{43}$$

and the parameters for  $M_{ij}$ ,  $N_{ij}$ ,  $P_{ij}$ ,  $Q_{ij}$  are given as follows: for  $G_{0,11}$ , we have

$$\begin{aligned}
 M_{11} &= 1, \\
 N_{11} &= \frac{\varepsilon}{\sqrt{\Delta_0^2 + \varepsilon^2}}, \\
 P_{11} &= \gamma_k + \varepsilon, \\
 Q_{11} &= \frac{-(\varepsilon^2 + \Delta_0^2 + \varepsilon\gamma_k)}{\sqrt{\Delta_0^2 + \varepsilon^2}};
 \end{aligned} \tag{44}$$

for  $G_{0,12}$ , we have

$$\begin{aligned}
 M_{12} &= 0, \\
 N_{12} &= \frac{-\Delta_0}{\sqrt{\Delta_0^2 + \varepsilon^2}}, \\
 P_{12} &= -\Delta_0, \\
 Q_{12} &= \frac{\Delta_0 \gamma_k}{\sqrt{\Delta_0^2 + \varepsilon^2}};
 \end{aligned} \tag{45}$$

for  $G_{0,13}$ , we have

$$\begin{aligned}
 M_{13} &= 0, \\
 N_{13} &= 0, \\
 P_{13} &= -\xi_k, \\
 Q_{13} &= \frac{\xi_k \varepsilon}{\sqrt{\Delta_0^2 + \varepsilon^2}};
 \end{aligned} \tag{46}$$

for  $G_{0,14}$ , we have

$$\begin{aligned}
 M_{14} &= 0, \\
 N_{14} &= 0, \\
 P_{14} &= 0, \\
 Q_{14} &= \frac{\xi_k \Delta_0}{\sqrt{\Delta_0^2 + \varepsilon^2}};
 \end{aligned} \tag{47}$$

for  $G_{0,22}$ , we have

$$\begin{aligned}
 M_{22} &= 1, \\
 N_{22} &= \frac{-\varepsilon}{\sqrt{\Delta_0^2 + \varepsilon^2}}, \\
 P_{22} &= \gamma_k - \varepsilon, \\
 Q_{22} &= \frac{-(\varepsilon^2 + \Delta_0^2 - \varepsilon\gamma_k)}{\sqrt{\Delta_0^2 + \varepsilon^2}}.
 \end{aligned} \tag{48}$$

for  $G_{0,23} = -G_{0,14}$ , we have

$$\begin{aligned}
 M_{23} &= 0, \\
 N_{23} &= 0, \\
 P_{23} &= 0, \\
 Q_{23} &= \frac{-\xi_k \Delta_0}{\sqrt{\Delta_0^2 + \varepsilon^2}};
 \end{aligned} \tag{49}$$

for  $G_{0,24}$ , we have

$$\begin{aligned} M_{24} &= 0, \\ N_{24} &= 0, \\ P_{24} &= \xi_k, \\ Q_{24} &= \frac{\xi_k \varepsilon}{\sqrt{\Delta_0^2 + \varepsilon^2}}; \end{aligned} \quad (50)$$

for  $G_{0,31} = G_{0,13}^*$

$$\begin{aligned} M_{31} &= 0, \\ N_{31} &= 0, \\ P_{31} &= -\xi_k^*, \\ Q_{31} &= \frac{\xi_k^* \varepsilon}{\sqrt{\Delta_0^2 + \varepsilon^2}}; \end{aligned} \quad (51)$$

for  $G_{0,32} = G_{0,23}^*$ , we have

$$\begin{aligned} M_{32} &= 0, \\ N_{32} &= 0, \\ P_{32} &= 0, \\ Q_{32} &= \frac{-\xi_k^* \Delta_0}{\sqrt{\Delta_0^2 + \varepsilon^2}}, \end{aligned} \quad (52)$$

for  $G_{0,33}$ , we have

$$\begin{aligned} M_{33} &= 1, \\ N_{33} &= \frac{\varepsilon}{\sqrt{\Delta_0^2 + \varepsilon^2}}, \\ P_{33} &= -(\gamma_k + \varepsilon), \\ Q_{33} &= \frac{\varepsilon^2 + \Delta_0^2 + \varepsilon \gamma_k}{\sqrt{\Delta_0^2 + \varepsilon^2}}; \end{aligned} \quad (53)$$

for  $G_{0,34}$ , we have

$$\begin{aligned} M_{34} &= 0, \\ N_{34} &= \frac{\Delta_0}{\sqrt{\Delta_0^2 + \varepsilon^2}}, \\ P_{34} &= -\Delta_0, \\ Q_{34} &= \frac{\Delta_0 \gamma_k}{\sqrt{\Delta_0^2 + \varepsilon^2}}; \end{aligned} \quad (54)$$

for  $G_{0,41} = G_{0,14}^*$ , we have

$$\begin{aligned} M_{41} &= 0, \\ N_{41} &= 0, \\ P_{41} &= 0, \\ Q_{41} &= \frac{\xi_k^* \Delta_0}{\sqrt{\Delta_0^2 + \varepsilon^2}}; \end{aligned} \quad (55)$$

for  $G_{0,42} = G_{0,24}^*$ , we have

$$\begin{aligned} M_{42} &= 0, \\ N_{42} &= 0, \\ P_{42} &= \xi_k^*, \\ Q_{42} &= \frac{\xi_k^* \varepsilon}{\sqrt{\Delta_0^2 + \varepsilon^2}}; \end{aligned} \quad (56)$$

for  $G_{0,44}$ , we have

$$\begin{aligned} M_{44} &= 1, \\ N_{44} &= \frac{-\varepsilon}{\sqrt{\Delta_0^2 + \varepsilon^2}}, \\ P_{44} &= -(\gamma_k - \varepsilon), \\ Q_{44} &= \frac{\varepsilon^2 + \Delta_0^2 - \varepsilon \gamma_k}{\sqrt{\Delta_0^2 + \varepsilon^2}}. \end{aligned} \quad (57)$$

- 
- [1] G. E. Volovik, Zh. Eksp. Teor. Fiz. **94**, 123 (1988) [Sov. Phys. JETP **67**, 1804 (1988)].  
[2] M. R. Zirnbauer, J. Math. Phys. **37**, 4986 (1996). A. Altland and M. R. Zirnbauer, Phys. Rev. B **55**, 1142 (1997).  
[3] A. Y. Kitaev, AIP Conf. Proc. **22**, 1134 (2009).  
[4] Shinsei Ryu, Andreas P. Schnyder, Akira Furusaki, and Andreas W. W. Ludwig, New J. Phys. **12**, 065010 (2010).  
[5] N. Read and D. Green, Phys. Rev. B **61**, 10267 (2000).  
[6] M. Sato, Yoshiro Takahashi and Satoshi Fujimoto, Phys.

- Rev. Lett. **103**, 020401 (2009).  
[7] Chuan-wei Zhang, Sumanta Tewari, Roman M. Lutchyn, and S. Das Sarma, Phys. Rev. Lett. **101**, 160401 (2008).  
[8] F. D. M. Haldane, Phys. Rev. Lett. **61**, 2015 (1988).  
[9] J. He, S. P. Kou, Y. Liang, S. P. Feng, Phys. Rev. B **83**, 205116 (2011).  
[10] J. He, Y. H. Zong, S. P. Kou, Y. Liang, S. P. Feng, Phys. Rev. B **84**, 035127 (2011).  
[11] J. He, Y. Liang, S. P. Kou, Phys. Rev. B **85**, 205107 (2012).

- [12] E. Taylor, A. Griffin, N. Fukushima and Y. Ohashi, Phys. Rev. A **74**, 063626 (2006).
- [13] M. Iskin and C. A. R. Sá de Melo, Phys. Rev. B **72**, 024512 (2005).
- [14] Erhai Zhao and Arun Paramekanti, Phys. Rev. Lett. **97**, 230404 (2006).
- [15] S. L. Zhu, B. Wang, L.-M. Duan, Phys. Rev. Lett. **98**, 260402 (2007).
- [16] L. B. Shao, Shi-Liang Zhu, Li. Sheng, D. Y. Xing, and Z. D. Wang, Phys. Rev. Lett. **101**, 246810 (2008).
- [17] C. Chin, et al, Rev. Mod. Phys. **82**, 1225-1286 (2010).
- [18] T. Köhler and K. Góral, Rev. Mod. Phys. **78**, 1311-1361 (2006).